Available online at www.sciencedirect.com
ScienceDirect
International Journal of Heat and Mass Transfer 50 (2007) 3767–3773
International Journal of HEAT and MASS TRANSFER
www.elsevier.com/locate/ijhmt

Geometry estimation of the furnace inner wall by an inverse approach

Chin-Ru Su, Cha'o-Kuang Chen *

Department of Mechanical Engineering, National Cheng Kung University, Tainan 70101, Taiwan, ROC

Received 27 August 2006; received in revised form 16 February 2007
Available online 26 April 2007

Abstract

The geometry of a furnace inner wall is estimated by an inverse method in this work. Based upon the concept of a virtual area, in the analysis process the heat conduction equation with boundary conditions was first discretized by a finite difference method to form a matrix equation. And then the linear least-squares error method was applied to determine the temperature of virtual boundary by inverse process. Finally, the geometry of the furnace inner wall can be obtained by direct process. Furthermore, the effects of the measurement errors, number of measurements and position of measurements on the deviation of geometry prediction are also discussed.

Keywords: Inverse problem; Inverse heat condition; Virtual area; Reverse matrix

1. Introduction

In heat conduction problem, if the boundary conditions, initial conditions and material properties are given, the temperature field in the system can be directly solved. This is the so-called well-posed problem and has the so-called direct solution. If the boundary conditions, initial conditions and material properties are unknown, but the temperature variation at some specific points in the system are given, the boundary conditions (boundary geometry), initial conditions and material properties can be inversely estimated. This is the so-called ill-posed problem [1] and has the so-called inverse solution. In inverse heat conduction problem, if the temperatures at some appropriate points on the surface or inside the solid are measured by a ultra-red optical thermometer or a thermocouple, the data can then be used to find initial values and boundary conditions (temperature or boundary geometry) or to analyze some significant parameters, such as thermal conductivity [2–4], surface heat flux [5–9] and internal energy source [10].

The inverse problem of undetermined geometry has been widely used in various industrial applications, for examples, the prediction of geometry of blast furnace inner wall, the prediction of crevice and pitting of furnace wall and the optimization of geometry (Chiang [11]). If the boundary geometry is unknown, the calculated region cannot be determined due to unknown boundary. Thus, the inverse problem becomes extremely complicated. In practical industrial applications the geometry of the blast furnace inner wall is in general represented by an isothermal curve of eutectic temperature of Fe–C system. So far the geometry of the furnace inner wall is mainly estimated by using some measured point temperatures based upon the theory in large steel factories. There are certain methods that are frequently used for the estimate of the geometry, e.g. estimation based on heat flux estimated by measured temperatures (Hitier [12]), estimation based on the relation between the measured temperatures and residual thickness of furnace wall (Suh [13]), and estimation by using the least-squares of errors between the measured and the estimated values based on optimum iterative theory (Yoshikawa [14]). As for the estimate of undetermined geometry

* Corresponding author. Tel.: +886 6 275 7575; fax: +886 6 234 2081.
E-mail address: ckchen@mail.ncku.edu.tw (C.-K. Chen).

0017-9310/$ - see front matter © 2007 Published by Elsevier Ltd.
doi:10.1016/j.ijheatmasstransfer.2007.02.024

Nomenclature

A	constant matrix constructed from thermal properties and space coordinates
B	coefficient matrix of **C**
Bi	Biot number, $h\bar{r}_o/k$
C	vector constructed from the unknown boundary conditions
E	product of $\mathbf{A}^{-1}$ and **B**
F	error function
h	heat transfer coefficients
k	thermal conductivity
R	reverse matrix
$\bar{r}$	dimensional radius of the cylinder
r	dimensionless radius of the cylinder
(r,θ)	cylindrical coordinate
$\overline{T}$	dimensional temperature
T	dimensionless temperature
T	temperature matrix
$T(r,\theta)$	temperature at each grid point (r,θ)

Greek symbols

Δr	increment of radial coordinate
$\Delta\theta$	increment of angular coordinate
ω	random number, $-1 < \omega < 1$
σ	measurement errors

Subscripts

est	estimated data
exact	exact temperature
i	index of radial coordinate, inner wall
j	index of angular coordinate
mea	measured data
m	number of unknown physical quantity
n	number of the linear equations after discretization
o	outer wall
p	number of measured points
∞	refers to ambient

of the boundary by inverse process, a general method was first developed in 1986 by Hsieh [15]. This method can also be applied for the estimation of non-linear geometry. A three-dimensional geometry was successfully predicted by the finite element methods proposed by Met [16] and Alexaudrou [17] in 1991. In 1997, Huang [18] estimated an irregular boundary shape by a conjugate gradient method and a Levenberg–Marquardt method using a boundary element approach. He found that the result obtained by the conjugate gradient method is better than that of Levenberg–Marquardt method. The former has many advantages include: (i) needs very short computer time; (ii) does not require a very accurate initial guess of the boundary shape; and (iii) needs less number of sensors. In 1999, Huang [19] further extended the inverse geometry problem to a multiple region domain in estimating time and space varying boundary configurations. This approach can be applied to nondestructive evaluation techniques and other problems such as frost thickness estimation in refrigeration systems. However, no matter what method is used, the number of measured points, the measurement locations, and the measurement errors are important in the process of geometry estimate.

This study proposed a new approach for the estimation of the geometry of a furnace inner wall on the basis of an inverse matrix method and a virtual area concept. In this proposed approach, the unknown geometry was first expressed as a function of temperature by a matrix equation constituted by rearrangement of the governing equation and boundary conditions. The actual geometry is then estimated by using the function of temperature. This study particularly emphasizes the effect of point numbers of measurement, measurement locations, and the measurement errors on the prediction of the unknown boundary.

2. Basic assumptions and mathematical model

2.1. The direct problem

Before the process is inversed, temperatures inside the system and on the furnace outer wall must be found by a direct process so that they can be adopted as the measured temperatures and the measurement errors needed for inverse estimation process. In this work a two-dimensional furnace wall system, as shown in Fig. 1, is considered. In this system the outer radius of the furnace is assumed to be a constant value of $\bar{r}_o$ and the inner radius $\bar{r}_i$ of the furnace is assumed to be dependent on the polar angle θ. To establish an appropriate physical model, some reasonable assumptions are presented. The temperature $\overline{T}_i$ in furnace is regarded as steady after a long time of operation and

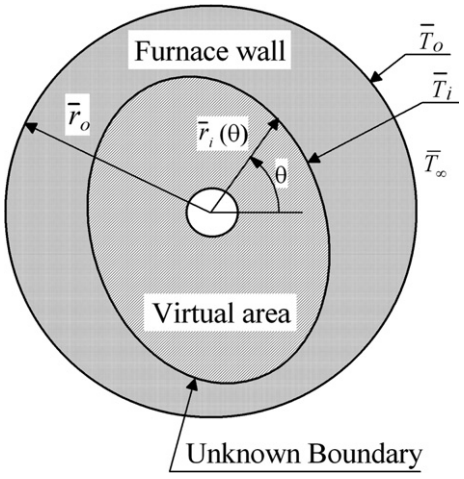

Fig. 1. The furnace wall system.

the thermal conductivity of furnace wall is taken as constant. The governing equation for the temperature, $\overline{T}(\bar{r},\theta)$, of the two-dimensional furnace wall system in steady state can be expressed as:

$$\frac{\partial^2\overline{T}(\bar{r},\theta)}{\partial\bar{r}^2}+\frac{1}{\bar{r}}\frac{\partial\overline{T}(\bar{r},\theta)}{\partial\bar{r}}+\frac{1}{\bar{r}^2}\frac{\partial^2\overline{T}(\bar{r},\theta)}{\partial\theta^2}=0 \tag{1}$$

The associated boundary conditions are given as

$$\overline{T}(\bar{r},\theta)=\overline{T}_i,\quad \bar{r}=\bar{r}_{\mathrm{i}} \tag{2}$$

$$-K\frac{\partial\overline{T}(\bar{r},\theta)}{\partial\bar{r}}=h(\overline{T}_{\mathrm{o}}-\overline{T}_\infty),\quad \bar{r}=\bar{r}_{\mathrm{o}} \tag{3}$$

The dimensionless parameters are taken as

$$r=\frac{\bar{r}}{\bar{r}_{\mathrm{o}}},\quad r_{\mathrm{i}}=\frac{\bar{r}_{\mathrm{i}}}{\bar{r}_{\mathrm{o}}},\quad r_{\mathrm{o}}=\frac{\bar{r}_{\mathrm{o}}}{\bar{r}_{\mathrm{o}}}=1,\quad T=\frac{\overline{T}-\overline{T}_\infty}{\overline{T}_i-\overline{T}_\infty},$$
$$Bi=\frac{h\bar{r}_{\mathrm{o}}}{k} \tag{4}$$

where Bi is Biot number. In this work the number is set to $Bi=2$. By plugging the dimensionless parameters into Eqs. (1)–(3), the governing equation and the boundary conditions become

$$\frac{\partial^2T(r,\theta)}{\partial r^2}+\frac{1}{r}\frac{\partial T(r,\theta)}{\partial r}+\frac{1}{r^2}\frac{\partial^2T(r,\theta)}{\partial\theta^2}=0 \tag{5}$$

$$T(r,\theta)=1,\quad r=r_{\mathrm{i}} \tag{6}$$

$$\frac{\partial T(r,\theta)}{\partial r}=-BiT(r,\theta),\quad r=r_{\mathrm{o}}=1 \tag{7}$$

Since the temperature is periodic in θ with a period 2π, one can have

$$T(r,\theta)=T(r,\theta+2\pi) \tag{8}$$

where $T(r,\theta)$ is the temperature at point (r,θ), which can then be obtained by using Eqs. (5)–(8).

2.2. The inverse process for the estimation of a furnace inner wall geometry

In the inverse process for obtaining the furnace inner wall geometry, the estimated region cannot be defined due to unknown boundary geometry $r_{\mathrm{i}}(\theta)$. Thus, the inverse process cannot be performed directly. A new method is then proposed based on a virtual area concept. As shown in Fig. 1, a virtual area is introduced inside the furnace $r<r_{\mathrm{i}}$. The thermal conductivity in this virtual area is the same as that in furnace wall. Except the virtual boundary, the outer boundary is assumed identical to the real system. The governing equation and basic assumptions of the virtual area are also assumed identical to the real system. Based on the conditions stated above, the geometry of furnace wall still cannot be directly found by the inverse process. The computed area is extended to the virtual boundary. For this reason, Eq. (6) should be replaced by

$$T(r,\theta)=T_{\mathrm{d}},\quad r=r_v \tag{9}$$

where $r=r_v$ is the virtual boundary.

The finite-difference method was first used to discretize the governing equation and boundary condition of Eqs. (5), (7)–(9). The result was shown as follows:

$$\frac{1}{(\Delta r)^2}(T_{i-1,j}-2T_{i,j}+T_{i+1,j})+\frac{1}{r}\frac{1}{2\Delta r}(T_{i+1,j}-T_{i-1,j})$$
$$+\frac{1}{r^2}\frac{1}{(\Delta\theta)^2}(T_{i,j-1}-2T_{i,j}+T_{i+1,j})=0 \tag{10}$$

$$T_{v,j}=T_{\mathrm{d}},\quad r=r_v \tag{11}$$

$$\frac{T_{I+1,j}-T_{I-1,j}}{2\Delta r}=-BiT_{I,j},\quad r=r_{\mathrm{o}} \tag{12}$$

$$T_{i,o}=T_{i,N} \tag{13}$$

In Eqs. (10)–(13), Δr and $\Delta\theta$ are the increment in dimensionless space coordinates; $T_{i,j}$ is the dimensionless temperature of grid point (i,j) in which subscript i and j are ith and jth grid point in r and θ coordinates, respectively; the subscript v in $T_{v,j}$ indicates the grid point at virtual boundary in r direction; T_{d} is the temperature of grid point (v,j) at virtual boundary. The subscript I represent the grids at outer surface, $r=r_{\mathrm{o}}$, and N denotes the number of grid point in θ direction. For inverse operation, Eqs. (10)–(13) must be rearranged, and the virtual system can be represented by the following matrix equation:

$$\mathbf{A}_{n\times n}\mathbf{T}_{n\times 1}=\mathbf{B}_{n\times m}\mathbf{C}_{m\times 1} \tag{14}$$

where $\mathbf{A}$ is a constant matrix which is a function of space increment Δr, $\Delta\theta$ and heat property; vector $\mathbf{T}$ is formed by the temperatures of measured points; vector $\mathbf{C}$ consists of temperature, $T_{\mathrm{d}(v,j)}$, of discrete points for determination; $\mathbf{B}$ is the coefficient matrix of $\mathbf{C}$; the n is the number of discretized linear equations; and m is the number of unknown boundary conditions.

We can rewrite Eq. (10) in the following form:

$$a_iT_{i-1,j}+b_iT_{i,j}+c_iT_{i+1,j}+d_iT_{i,j-1}+e_iT_{i,j+1}=0 \tag{15}$$

where a_i-e_i are the constant parameters constructed from the spatial coordinates of the system. Therefore, the elements of each matrix in the linear matrix Eq. (14) can be expressed as

$$\mathbf{A}=\begin{bmatrix}\overline{\mathbf{A}}_1 & \ddots & \ddots & & \mathbf{0}\\ \ddots & \ddots & c_i\mathbf{I} & \mathbf{0} & \\ \ddots & a_i\mathbf{I} & \overline{\mathbf{A}}_i & c_i\mathbf{I} & \ddots\\ & \mathbf{0} & a_i\mathbf{I} & \ddots & \ddots\\ \mathbf{0} & & \ddots & 2\mathbf{I} & \overline{\mathbf{A}}_I\end{bmatrix}_{(I\cdot J)\times(I\cdot J)},$$

$$\overline{\mathbf{A}}_i=\begin{bmatrix}\ddots & & \ddots & & d_i\\ \ddots & \ddots & \ddots & 0 & \\ \ddots & d_i & b_i & e_i & \ddots\\ & 0 & \ddots & \ddots & \ddots\\ e_i & & \ddots & & \ddots\end{bmatrix}_{J\times J}$$

$$\overline{\mathbf{A}}_I = \begin{bmatrix} \ddots & & \ddots & & d_I \\ \ddots & \ddots & \ddots & 0 & \\ \ddots & d_I & sur & e_I & \ddots \\ & 0 & \ddots & \ddots & \ddots \\ e_I & & \ddots & & \ddots \end{bmatrix}_{J\times J}$$

where $\mathbf{I}$ is an identity matrix, $\mathbf{0}$ is a zero matrix, $sur = b_I - 2c_I Bi\Delta r$

$$\mathbf{T} = [\,\overline{\mathbf{T}}_1 \quad \cdots \quad \overline{\mathbf{T}}_i \quad \cdots \quad \overline{\mathbf{T}}_I\,]^{\mathrm{T}},$$
$$\overline{\mathbf{T}}_i = [\,T_{i,1} \quad \cdots \quad T_{i,j} \quad \cdots \quad T_{i,J}\,]^{\mathrm{T}}$$
$$\mathbf{B} = [\,\overline{\mathbf{B}}_1 \quad \mathbf{0} \quad \cdots \quad \cdots \quad \mathbf{0}\,]^{\mathrm{T}}_{J\times(I\cdot J)},$$
$$\overline{\mathbf{B}}_1 = -0.5\mathbf{I},$$
$$\mathbf{C} = [\,T_{v,1} \quad \cdots \quad T_{v,j} \quad \cdots \quad T_{v,J}\,]^{\mathrm{T}}$$

A major advantage of the proposed inverse approach is that the construction of the linear inverse model given in Eq. (14) requires no explicit assumptions regarding the functional forms of the unknown geometry. Finally, the measured temperatures are substituted into the inverse model of Eq. (14), which can then be solved using the following procedure:

Suppose that the estimated conditions of $\mathbf{C}_{\mathrm{est}}$ can be obtained from the given estimated temperatures, $\mathbf{T}_{\mathrm{est}}$, then:

$$\mathbf{A}\mathbf{T}_{\mathrm{est}} = \mathbf{B}\mathbf{C}_{\mathrm{est}} \tag{16}$$

The matrix $\mathbf{A}$ has an inverse matrix $\mathbf{A}^{-1}$ due to the existence of the unique solution for the problem. Eq. (16) can be further re-arranged and expressed as

$$\mathbf{T}_{\mathrm{est}} = \mathbf{A}^{-1}\mathbf{B}\mathbf{C}_{\mathrm{est}} = \mathbf{E}\mathbf{C}_{\mathrm{est}} \tag{17}$$

where $\mathbf{E} = \mathbf{A}^{-1}\mathbf{B}$. The total number of the linear equation groups in the above formula is n. The equation corresponding to the measured value of $(\mathbf{T}_{\mathrm{mea}})_{p\times 1}$ can be taken out and re-expressed as

$$\mathbf{T}_{p\times 1} = (\mathbf{A}^{-1}\mathbf{B})_{p\times m}\mathbf{C}_{m\times 1} \tag{18}$$

where p is the number of measured values. By comparing the difference between the measured value $\mathbf{T}_{\mathrm{mea}}$ and the estimated value $\mathbf{T}_{\mathrm{est}}$, the error function F can be expressed as

$$\mathbf{F} = (\mathbf{T}_{\mathrm{est}} - \mathbf{T}_{\mathrm{mea}})^{\mathrm{T}}(\mathbf{T}_{\mathrm{est}} - \mathbf{T}_{\mathrm{mea}}) \tag{19}$$

By plugging Eg. (17) into (19), one can obtain

$$\begin{aligned}\mathbf{F} &= (\mathbf{E}\mathbf{C}_{\mathrm{est}} - \mathbf{T}_{\mathrm{mea}})^{\mathrm{T}}(\mathbf{E}\mathbf{C}_{\mathrm{est}} - \mathbf{T}_{\mathrm{mea}}) \\ &= \mathbf{C}^{\mathrm{T}}_{\mathrm{est}}\mathbf{E}^{\mathrm{T}}\mathbf{E}\mathbf{C}_{\mathrm{est}} - \mathbf{T}^{\mathrm{T}}_{\mathrm{mea}}\mathbf{E}\mathbf{C}_{\mathrm{est}} - \mathbf{C}^{\mathrm{T}}_{\mathrm{est}}\mathbf{E}^{\mathrm{T}}\mathbf{T}_{\mathrm{mea}} + \mathbf{T}^{\mathrm{T}}_{\mathrm{mea}}\mathbf{T}_{\mathrm{mea}}\end{aligned} \tag{20}$$

This error function can then be minimized by differentiating $\mathbf{F}$ with respect to $\mathbf{C}_{\mathrm{est}}$ as

$$\frac{\partial \mathbf{F}}{\partial \mathbf{C}_{\mathrm{est}}} = 0 \tag{21}$$

Following a process of mathematical manipulation, it can be shown that

$$\mathbf{E}^{\mathrm{T}}\mathbf{E}\mathbf{C}_{\mathrm{est}} = \mathbf{E}^{\mathrm{T}}\mathbf{T}_{\mathrm{mea}} \tag{22}$$

Hence, vector $\mathbf{C}_{\mathrm{est}}$ can then be solved as follows:

$$\mathbf{C}_{\mathrm{est}} = (\mathbf{E}^{\mathrm{T}}\mathbf{E})^{-1}\mathbf{E}^{\mathrm{T}}\mathbf{T}_{\mathrm{mea}} = \mathbf{R}\mathbf{T}_{\mathrm{mea}} \tag{23}$$

where $\mathbf{R} = (\mathbf{E}^{\mathrm{T}}\mathbf{E})^{-1}\mathbf{E}^{\mathrm{T}}$ is called a reverse matrix. Therefore, when a measured value of $\mathbf{T}_{\mathrm{mea}}$ is given, an optimum estimated value C_{est} for the temperature of inner wall in virtual area can be obtained by the method of linear least-squares of errors.

The major objective of this study is to estimate the geometry of the furnace inner wall. The temperature fields of the furnace wall and the virtual area can be obtained by the direct method by using the heat conduction Eq. (5) and the boundary conditions consisting of the temperature $T(1,\theta)$ of furnace outer wall and the estimated temperature C_{est} of inner wall of virtual area obtained from Eq. (23). The curve of the isothermal line, $T(r,\theta) = 1$, in the temperature field is just the undetermined geometry of the furnace inner wall. It should be noted that if the positions of the isothermal curve do not lie on the grid points of estimation, the correct positions of the isothermal curve should be determined by interpolation.

3. Results and discussion

The result of the inverse prediction is in general affected by the measurement number of points, and the measurement locations, and the measurement errors. In order to verify the appropriateness of the method proposed in this study, various points of measurement, and positions of measurement are used to predict the undetermined geometry and the results are used to compare with each other. Because the real temperature measurement is not carried out in this study, the temperatures needed for inverse estimation are taken from the temperature field obtained by the direct solution. In practice, the temperature measurements always contain some degree of error, whose magnitude depends upon the particular measuring method employed. Therefore, the simulated temperature measurements adopted in the current inverse problem are also considered to include measurement errors. For reasons of practicality, the present study adds a random error noise to the exact temperature values computed from the direct problem. Hence, the measured dimensionless temperature, T_{mea}, is expressed as

$$T_{\mathrm{mea}} = T_{\mathrm{exact}}(1 + \sigma\omega) \tag{24}$$

where T_{exact} is the field temperature of the measured points obtained from the direct process, ω is a random variable generated by the DRNNOR subroutine of the IMSL [20], and σ is the standard deviation of the measurement error. For normally distributed random errors, the probability of a random value, ω, lying in the range $-2.576 < \omega < 2.576$ is 99% [10].

3.1. Case 1: The effect of measurement error

The number of measured points and their locations on the furnace wall are given in Fig. 2. The function of the geometry of furnace inner wall is assumed as

$$r_i(\theta) = 0.6 + 0.1\sin(\theta + 45^\circ) \tag{25}$$

The temperature field of the furnace wall can be directly found from heat conduction Eq. (5), boundary conditions Eqs. (6)–(8), and the geometry of the furnace inner wall. In order to meet the constraint conditions in inverse process, the exact temperature T_{exact} of 10 measured points are uniformly distributed on $r = 0.95$, as shown in Fig. 2. These data are used to obtain simulated temperature T_{mea} with certain measurement errors given by Eq. (24). The temperature distribution on the inner boundary of the virtual area can then be obtained by Eq. (23). The field temperature of the virtual area and the furnace wall can finally be obtained by the traditional direct process. Fig. 3 shows the field temperature of the virtual area and

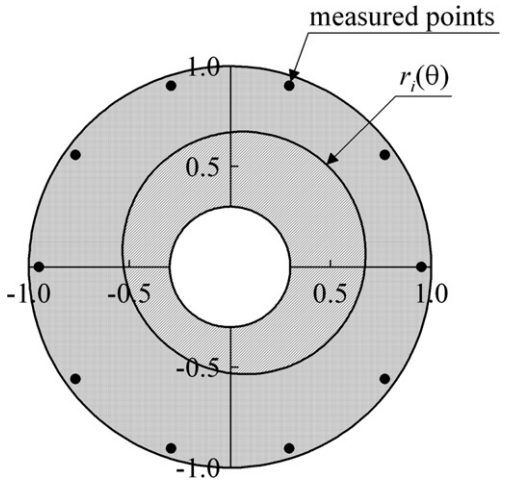

Fig. 2. Furnace with a sinusoidal inner wall and positions of measured points.

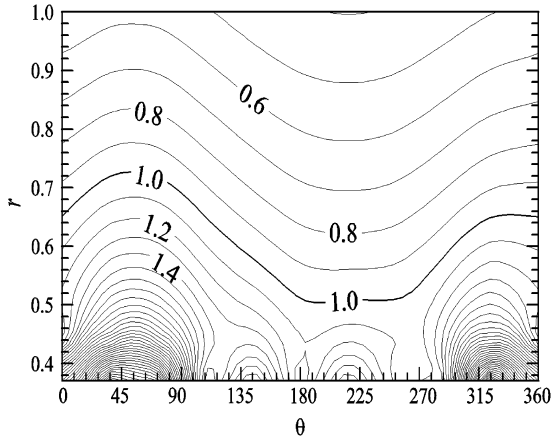

Fig. 3. Temperature filed of virtual area and furnace wall with measurement error $\sigma = \pm 5\%$.

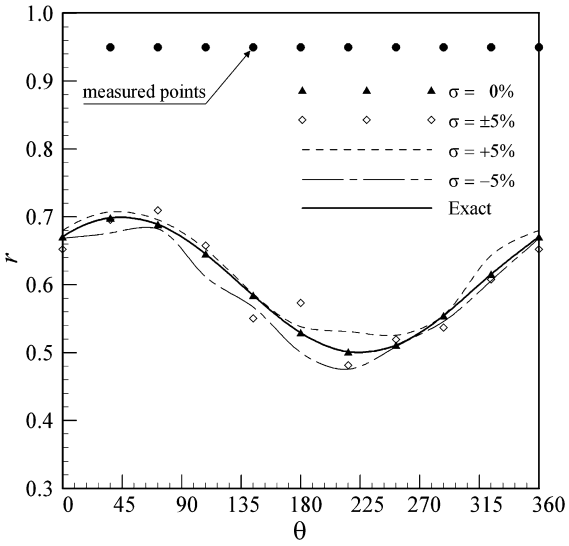

Fig. 4. Effects of various measurement errors on the prediction of the geometry of furnace inner wall.

furnace wall with a measurement error bound of $\sigma = \pm 5\%$. In Fig. 3 the curve of the isothermal line, $T(r_i, \theta) = 1$, is a undetermined geometry of the furnace inner wall. On top of the curve is the furnace wall. Below the curve is the virtual area. Fig. 4 shows the effects of various measurement errors on the geometry prediction of the furnace inner wall. If no measurement error is given, i.e. $\sigma = 0$, the result of the inverse solution coincides exactly with the original geometry. This obviously indicates that under the condition of no measurement error, the exact solution of Eq. (25) can be obtained by the method proposed in this work. As measurement error exists, the predicted geometry will deviate from the exact solution, as shown in Fig. 4. As a measurement error bound is given as 5%, the furnace wall has a relatively smaller thickness. This means that the geometry is over-estimated. On the other hand, a contrary result will be obtained as a measurement error bound of -5% is given. These results manifest that if the measurement error is positive, a larger measurement value will be obtained. If the temperature of furnace inner wall is fixed, only thinner furnace wall can obtain a relatively higher measured value. The reason stated above is also suitable for negative measurement error. Thus, these results are coincident exactly with the physical principle. Additionally, as a measurement error bound of $\sigma = \pm 5\%$ is given, the predicted curve is slightly undulated as compared to the exact solution.

3.2. Case 2: The effect of positions of measurement points

Fig. 5 and 6 show the distribution of measured point locations and the result of inverse modeling process, respectively. The geometry of the furnace inner wall in this example is given as an ellipse with a long axis of 0.7 and a short axis of 0.5. This can be expressed as

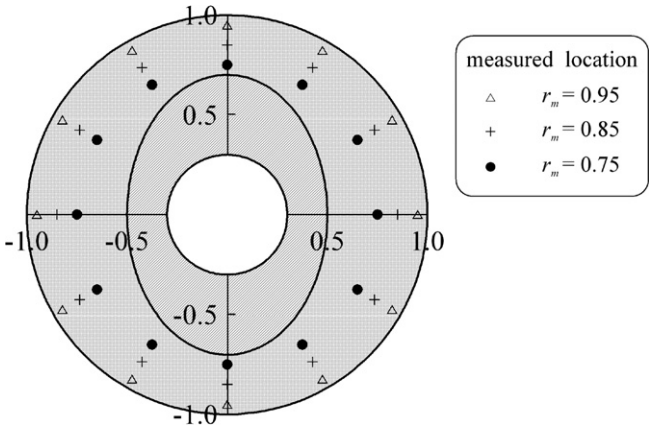

Fig. 5. Furnace with an elliptical inner wall and positions of measured points.

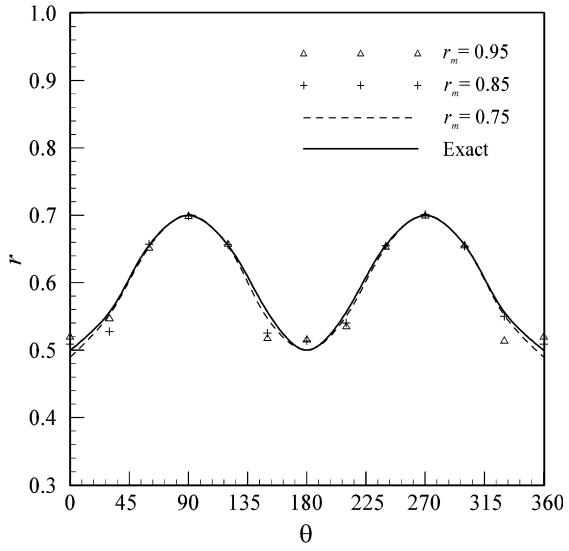

Fig. 6. Effects of various measured positions on the prediction of the geometry of the furnace inner wall with measurement error $\sigma = \pm 0.5\%$.

$$r_i(\theta) = \sqrt{(0.5\cos\theta)^2 + (0.7\sin\theta)^2} \tag{26}$$

In this study, the error bound of measurement is assumed to be $\sigma = \pm 0.5\%$. Twelve measured points are located on furnace wall at $r_m = 0.95$, 0.85 and 0.75, respectively. The predicted results are shown in Fig. 6. It is found that the predicted result is better for measured points nearest to inner wall. The errors of predicted values increase as the distance between measured points and the inner wall is increased. As for the predicted curve of the measured points at $r_m = 0.95$, the error of the predicted value for the measured point near $\theta = 0^\circ$ and $\theta = 180^\circ$ is clearly larger than those of other measured points. This result can be attributed to that the farther the distance between measured points and the inner wall, the smaller the measured temperature. It means that the effect of measurement error on the prediction is larger than the geometry of the inner wall. Anyway, even if the measured points are quite near the outer wall, e.g. at $r_m = 0.95$, the predicted result is still quite well. Therefore, it is clear that no matter how the positions of measured points distributed, the undetermined geometry of the furnace inner wall can be successfully estimated by the proposed method presented in this work.

3.3. Case 3: The effect of number of the measured points

In Fig. 7, the geometry of furnace inner wall is assumed to be an eccentric ellipse. In order to study the effect of number of measured points on prediction accuracy, the measured points in this example are given as in Fig. 7. Fig. 8 shows the predicted result of 12 measured points at $r_m = 0.95$ with measurement error bound $\pm 5\%$. It is found that the predicted values for the measured points at $150^\circ < \theta < 240^\circ$ are undulated as compared to the exact solution. When the number of measured points is increased to 24, the predicted results are clearly improved since the measured points are far from the inner wall. As the number

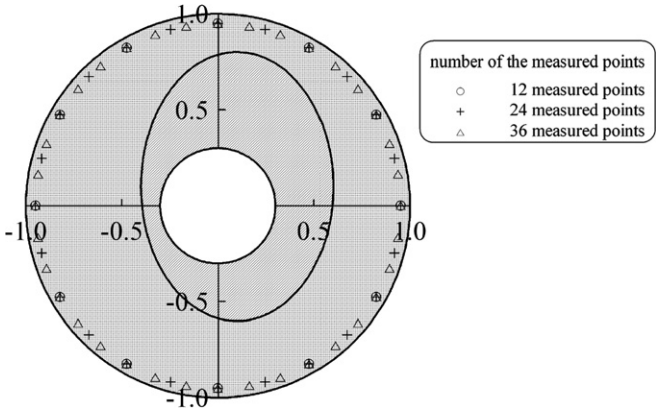

Fig. 7. Furnace with an eccentrically elliptical inner wall and positions of measured points.

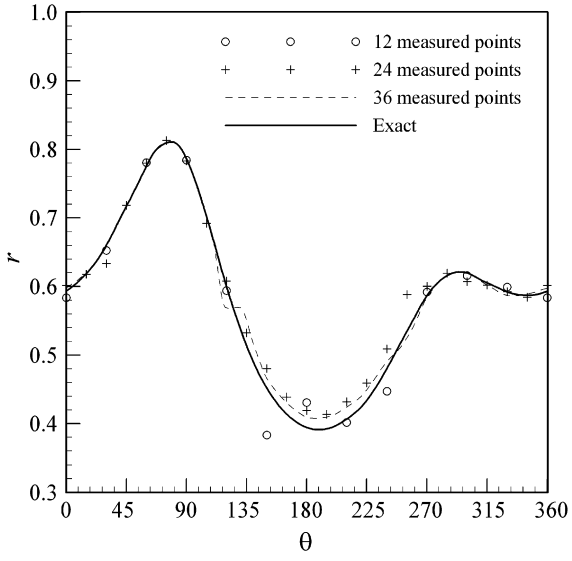

Fig. 8. Effects of various number of measured points on the prediction of the geometry of the furnace inner wall with measurement error $\sigma = \pm 5\%$.

of measured points is increased to 36, the predicted results are almost coincident with the exact solution of the measured points. This means that the effect of measurement error on geometry prediction is diminished as the number of measured points is increased, or the increase of reference data in inverse process. If the measurement equipment is not good enough to minimize measurement errors, the method by increasing number of measured points can be used to enhance the accuracy of prediction in inverse process.

4. Conclusion

Since the assumption on the form of initial solution is not necessary, the inverse problem can be analyzed directly. No iteration is needed in the method of linear least-squares of errors proposed in this work. The proposed method fits for all problems in which the geometry is complicated and undetermined beforehand. The results of the numerical verification show that the geometry of furnace inner wall, regardless of sinusoidal, elliptical or eccentrically elliptical shapes, can be successfully estimated by the proposed method. Furthermore, the results also show that the deviation of geometry prediction is increased as the distance between measured points of the undetermined geometry and the measurement errors is increased. The method proposed by this work has many advantages including: (i) the time for computational operation is relatively short; (ii) the number of measured points needed for the estimation of geometry is little; and (iii) the positions of the measured points almost do not affect the result of estimation. Therefore, it is proved to be an excellent approach for real-world applications with high accuracy and efficiency.

References

[1] A.N. Tikhnov, V.Y. Arsenin, Solution of Ill-posed Problems, V.H. Winston, Washington, DC, 1977.
[2] C.Y. Yang, Linear inverse model for the temperature-dependent thermal conductivity determination in one-dimensional problems, Appl. Math. Modell. 22 (1) (1998) 1–9.
[3] C.Y. Yang, Estimation of the temperature-dependent thermal conductivity in inverse heat conduction problems, Appl. Math. Modell. 23 (6) (1999) 469–478.
[4] J.H. Lin, C.K. Chen, Y.T. Yang, Inverse method for estimating thermal conductivity in one-dimensional heat conduction problems, AIAA J. Thermo-Phys. Heat Transfer 15 (1) (2001) 34–41.
[5] T.J. Martin, G.S. Dulikravich, Finding unknown surface temperatures and heat fluxes in steady heat conduction, IEEE Trans. Component. Pack. Manuf. Technol. Part A 18 (3) (1995) 540–545.
[6] P.T. Hsu, Y.T. Yang, C.K. Chen, Simultaneously estimating the initial and boundary conditions in a two-dimensional hollow cylinder, Int. J. Heat Mass Transfer 41 (1) (1998) 219–227.
[7] G.R. Warrier, L.C. Witte, On the application of the hyperbolic heat equation in transient heat flux estimation during flow film boiling, Numer. Heat Transfer, Part A 35 (4) (1999) 343–359.
[8] C.C. Wang, C.K. Chen, Three-Dimensional inverse heat transfers analysis during grinding process, Proc. Inst. Mech. Eng., Part C: J. Mech. Eng. Sci. 216 (2) (2002) 199–212.
[9] H.Y. Jang, P.C. Tuan, T.C. Chen, T.S. Chen, Input estimation method combined with the finite-element scheme to solve IHCP hollow-cylinder inverse heat conduction problems, Numer. Heat Transfer, Part A 50 (3) (2006) 263–280.
[10] A.J. Silva Neto, M.N. Özisik, Inverse problem of simultaneously estimating the timewise-varying strengths of two plane heat sources, J. Appl. Phys. 73 (5) (1993) 2132–2137.
[11] C.C. Chiang, S.K. Chou, Inverse geometry design problem in optimizing hull surfaces, J. Ship Res. 42 (2) (1998) 79–85.
[12] B. Hitier, Calculation and conclusions based on temperature measurements in the bottom of No. 1 blast furnace of CSC, Savoie Refractories, France, private communication, 1997.
[13] Y.K. Suh, C.M. Cho, H.K. Lee, Evaluation of mathematical model for estimating refractory wear and solidified layer in the blast furnace hearth, in: Proceedings of the First International Congress of Science and Technology of Iron Marking, ISIJ, Sendai, Japan, 1994, pp. 223–228.
[14] F. Yoshikawa, S. Nigo, S. Kiyohara, S. Taguchi, H. Takahashi, M. Ichimiya, Estimation of refractory wear and solidified layer distribution in the blast furnace hearth and its application to the operation, Iron Steel (1987) 2068–2075.
[15] C.K. Hsieh, A.J. Kassab, A general method for the solution of inverse heat conduction problems with partially unknown system geometries, Int. J. Heat Mass Transfer 29 (1) (1986) 47–58.
[16] L. Met, X.A. Wang, X Y. Meng, Finite element method to an inverse problem of three-dimensional heat conduction with partially unknown system geometries, in: Proceedings of the International Conference on Numerical Methods in Thermal Problems, 1991, pp. 1514.
[17] A.N. Alexandrou, Inverse finite element method for directly formulated free and moving boundary problems, Comput. Modell. Free Moving Bound. Prob. (1991) 149–163.
[18] C.H. Huang, B.H. Chao, An inverse geometry problem in identifying irregular boundary configurations, Int. J. Heat Mass Transfer 40 (9) (1997) 2045–2053.
[19] C.H. Huang, H.M. Chen, Inverse geometry problem of identifying growth of boundary shapes in a multiple region domain, Numer. Heat Transfer, Part A 35 (4) (1999) 435–450.
[20] IMSL User's Manual, 1985, Math Library Version 1.0, IMSL Library Edition 10.0, IMSL, Houston, TX.